

Nuclear enhanced power corrections to DIS structure functions

Xiaofeng Guo^{1*}, Jianwei Qiu², and Wei Zhu^{3,4}

¹*Department of Physics and Astronomy, University of Kentucky,
Lexington, Kentucky 40506, USA*

²*Department of Physics and Astronomy, Iowa State University
Ames, Iowa 50011, USA*

³*Department of Physics, East China Normal University
Shanghai 200062, China*

⁴*International Institute of Theoretical and Applied Physics, Iowa State University
Ames, Iowa 50011, USA*

(October 1, 2001)

Abstract

We calculate nuclear enhanced power corrections to structure functions measured in deeply inelastic lepton-nucleus scattering in Quantum Chromodynamics (QCD). We find that the nuclear medium enhanced power corrections at order of $O(\alpha_s/Q^2)$ enhance the longitudinal structure function F_L , and suppress the transverse structure function F_1 . We demonstrate that strong nuclear effects in σ_A/σ_D and R_A/R_D , recently observed by HERMES Collaboration, can be explained in terms of the nuclear enhanced power corrections.

PACS Numbers: 24.85.+p, 13.85.Qk, 12.38.Bx, 11.80.La

Typeset using REVTeX

*Current email address: gxf@iastate.edu.

Recently, a strong nuclear dependence in lepton-nucleus deeply inelastic scattering (DIS) was observed by HERMES collaboration [1]. HERMES data show a large nuclear enhancement in the longitudinal cross section when Bjorken x_B is small. The ratio of longitudinal cross sections σ_L^A/σ_L^D measured by HERMES Collaboration was as large as 2 for scattering off a ^{14}N target. On the other hand, due to nuclear shadowing in the small x region, the ratio of the transverse cross section σ_T^A/σ_T^D is much less than 1, which leads to a very large nuclear enhancement in a double ratio $(\sigma_L^A/\sigma_T^A)/(\sigma_L^D/\sigma_T^D)$ [1]. The anomalous nuclear effects observed by HERMES have generated lots of interests [2]. In this Letter, we calculate the nuclear dependence of the DIS cross sections (or DIS structure functions) at low Q^2 in terms of medium enhanced power corrections in QCD perturbation theory, and provide our understanding of HERMES data.

For low energy fixed target DIS processes, like HERMES experiment, we neglect a small contribution from vector boson Z and take the one-photon exchange approximation. Like other DIS experiments, HERMES experiment measures inclusive lepton-nucleus cross sections as a function of x_B and virtual photon's invariant mass square Q^2 [1]

$$\frac{d\sigma_{\ell h}}{dx_B dQ^2} = \frac{\sigma_{\text{Mott}}}{EE'} \frac{\pi F_2(x_B, Q^2)}{\epsilon x_B} \left[\frac{1 + \epsilon R(x_B, Q^2)}{1 + R(x_B, Q^2)} \right], \quad (1)$$

where σ_{Mott} represents an elastic cross section for lepton scattering from a point charge, and E and E' are incoming and scattered lepton energy, respectively. The parameter ϵ is given by [1]

$$\epsilon = \frac{4(1-y) - Q^2/E^2}{4(1-y) + 2y^2 + Q^2/E^2}, \quad (2)$$

where $y = (E - E')/E$. The $R(x_B, Q^2)$ in Eq. (1) is the ratio of longitudinal to transverse DIS cross sections $R = \sigma_L/\sigma_T$. When $x_B < 0.03$, HERMES data on the ratio of inclusive DIS cross sections from nucleus A and deuterium $D(=^2\text{H})$, σ_A/σ_D , show major differences from what have been measured by other experiments in terms of the dependences on x_B , Q^2 , and ϵ [1]. When x_B decreases, the ratio falls steeply, and is much smaller than what was measured by other experiments. When Q^2 increases, the ratio is not only small but also decreases. On the other hand, the ratio increases when ϵ increases. Why HERMES data is so different from other data in the small x_B region?

From Eq. (1), the ratio of inclusive DIS cross sections from nucleus A and deuterium $D(=^2\text{H})$ can be expressed as [1]

$$\frac{\sigma_A}{\sigma_D} = \frac{F_2^A}{F_2^D} \frac{(1 + \epsilon R_A)(1 + R_D)}{(1 + R_A)(1 + \epsilon R_D)}, \quad (3)$$

where R_A and R_D represent the ratio of σ_L/σ_T for nucleus A and deuterium D . HERMES Collaboration shows that the ratio of F_2^A/F_2^D extracted from its data is consistent with the previous measurements, and attributes the differences in the ratio of cross sections, σ_A/σ_D , to the strong nuclear dependence in R_A/R_D [1]. At the same x_B , the key difference between HERMES data and other data is the range of Q^2 and ϵ . When x_B is small, the Q^2 of HERMES data is much smaller than that of other data sets. It is then natural to investigate the role of $1/Q^2$ type power corrections to the ratio of the DIS cross sections, R .

When energy exchange of the collision, Q , is much larger than the typical momentum scale of the hadron wave function, the DIS process is dominated by a single hard collision between the lepton and a quark via the virtual photon, as shown in Fig. 1(a). The corresponding cross section is given by the probability to find a quark within a hadron times an elastic cross section between this quark and the incoming lepton. QCD radioactive corrections to such a single parton scattering picture are well-defined [3]. However, in a large nucleus, partons from different nucleons can interact with each other before the hard collision takes place, as shown in Fig. 1(b), or interact with the scattered quark after the hard collision, as shown in Fig. 1(c). Just like the process in Fig. 1(a), leading contributions from the process shown in Fig. 1(b) is dominated by the phase space where the quark of momentum k is pinched to be on-mass shell. That is, the multiparton interactions from different nucleons are separated from the hard collision by a “long” time scale. Therefore, such multiparton interactions are internal to the nucleus, and do not affect the short-distance hard collision between the quark and the virtual photon. On the other hand, such interactions are responsible for the differences between the parton distribution in a nucleus and that in a free nucleon [4]. Because of the leading twist nature of the operators defining the parton distributions in a nucleus, and the fact that F_2 is dominated by the contributions from the parton distributions, the ratio of F_2^A/F_2^D has a small Q^2 dependence [5,6].

Unlike the parton momentum k in Fig. 1(b), the parton momentum k' in Fig. 1(c) is not pinched after we square the scattering amplitude due to different gluon momenta in the amplitude and its complex conjugate [7]. The integration of the unpinched parton momentum k' can be deformed away from the $k'^2 = 0$, and the quark-gluon interaction in Fig. 1(c) is a part of the hard collision. Because of the extra interactions with the scattered quark, physical contributions from such multiparton scattering are suppressed by inverse powers of Q^2 , known as the high twist contributions [8–10]. Although their contributions to the DIS structure functions are normally small in lepton-hadron collisions, such power corrections can be important in the nuclear collisions because of the enhancement of nuclear size [11]. In the rest of this Letter, we show that the power corrections caused by the type of multiparton interactions shown in Fig. 1(c) are responsible for the features seen in the HERMES data.

In terms of DIS structure functions, $F_1(x_B, Q^2)$ and $F_2(x_B, Q^2)$, the ratios of the DIS cross sections can be expressed as [12]

$$\frac{\sigma_L}{\sigma_T} = \frac{1}{2x_B F_1} \left[\left(1 + \frac{4m_N^2 x_B^2}{Q^2} \right) F_2 - 2x_B F_1 \right] \equiv \frac{F_L}{2F_1} \quad (4)$$

where m_N is nucleon mass, and the longitudinal structure function F_L is defined as ¹

$$F_L = \frac{1}{x_B} \left[\left(1 + \frac{4m_N^2 x_B^2}{Q^2} \right) F_2 - 2x_B F_1 \right] \approx \frac{1}{x_B} [F_2 - 2x_B F_1] \quad (5)$$

when $x_B \ll 1$ or $m_N^2 \ll Q^2$. Let us introduce two projection operators,

¹Our definition of F_L in Eq. (5) differs by a factor of $1/x_B$ from that in Ref. [1].

$$e_L^{\mu\nu} = \frac{1}{Q^2} [q^\mu + 2x_B p^\mu] [q^\nu + 2x_B p^\nu], \quad (6)$$

$$e_T^{\mu\nu} = \frac{1}{p \cdot q} [p^\mu q^\nu + q^\mu p^\nu] + \frac{2x_B}{p \cdot q} p^\mu p^\nu - g^{\mu\nu}, \quad (7)$$

where q^μ is virtual photon's four-momentum with $q^2 = -Q^2$. The DIS hadronic tensor $W^{\mu\nu}$ can be then expressed as [9]

$$W^{\mu\nu}(x_B, Q^2) = \frac{1}{2} [e_L^{\mu\nu} F_L(x_B, Q^2) + e_T^{\mu\nu} 2 F_1(x_B, Q^2)]. \quad (8)$$

Therefore, we can extract the DIS structure functions from the hadronic tensor as

$$F_L(x_B, Q^2) = 2 e_L^{\mu\nu} W_{\mu\nu}(x_B, Q^2), \quad \text{and} \quad F_1(x_B, Q^2) = \frac{1}{2} e_T^{\mu\nu} W_{\mu\nu}(x_B, Q^2). \quad (9)$$

At the lowest order, the DIS structure functions in lepton-nucleus collisions are given by

$$F_L^A(x_B, Q^2) = 0, \quad (10)$$

$$F_1^A(x_B, Q^2) = \frac{1}{2x_B} F_2^A(x_B, Q^2) = \frac{1}{2} \sum_q e_q^2 \phi_{q/A}(x_B, Q^2), \quad (11)$$

where \sum_q runs over all quark and antiquark flavors and e_q is corresponding fractional charge. The $\phi_{q/A}$ is an effective quark distribution in a nucleus of atomic number A , which is normalized by dividing the A .

The lowest order power corrections to the DIS structure functions are given by the Feynman diagrams in Fig. 2, plus the diagrams with four-quark lines instead of two-quark-two-gluon lines [9]. Since we are interested in the medium size enhanced power corrections, we neglect the four-quark processes [11]. In Fig. 2, the quark lines with a short bar are special quark propagators, which are equal to the normal quark propagators with the leading twist contributions removed [9]. The diagrams with special quark propagators in Fig. 2 are important to preserve the electromagnetic current conservation at the level of power corrections. Feynman rules for the special quark propagators are given in Refs. [9,13]. In the light-cone gauge of the strong interaction, contributions to the hadronic tensor from the diagrams in Fig. 2 can be factorized as [11]

$$W_{qA}^{\mu\nu}(x_B, Q^2) = \frac{1}{4\pi} \int dx dx_1 dx_2 T_{qA}(x, x_1, x_2) H_{qA}^{\mu\nu}(x, x_1, x_2, q). \quad (12)$$

The hadronic matrix element T_{qA} is given by

$$\begin{aligned} T_{qA}(x, x_1, x_2) &= \left(\frac{1}{x - x_1} \right) \left(\frac{1}{x - x_2} \right) \int \frac{dy^-}{2\pi} \frac{dy_1^-}{2\pi} \frac{dy_2^-}{2\pi} e^{ix_1 p^+ y^-} e^{i(x-x_1)p^+ y_1^-} e^{-i(x-x_2)p^+ y_2^-} \\ &\times \langle P_A | \bar{\psi}(0) \frac{\gamma^+}{2} F^{+\alpha}(y_2^-) F_\alpha^+(y_1^-) \psi(y^-) | P_A \rangle, \end{aligned} \quad (13)$$

where $p \equiv P_A/A$ is averaged momentum per nucleon. In deriving T_{qA} , we used $F^{+\alpha}(y^-) = n^\rho \partial_\rho A^\alpha(y^-)$ in the light-cone gauge. The partonic part $H_{qA}^{\mu\nu}$ is given by the Feynman diagrams in Fig. 2 with the quark lines contracted by $\frac{1}{2} \gamma \cdot p$ and gluon lines contracted by $\frac{1}{2} d_{\alpha\beta}$.

The transverse tensor $d_{\alpha\beta} = -g_{\alpha\beta} + \bar{n}_\alpha n_\beta + n_\alpha \bar{n}_\beta$ with two lightlike vectors, $\bar{n}^\mu = \delta^{\mu+}$ and $n^\mu = \delta^{\mu-}$. After contracting with the projection operators, we obtain [9]

$$e_L^{\mu\nu} H_{\mu\nu}^{qA}(x_B, Q^2) = 4 e_q^2 \left(\frac{4\pi^2 \alpha_s}{3} \right) \frac{1}{Q^2} \delta(x - x_B), \quad (14)$$

$$e_T^{\mu\nu} H_{\mu\nu}^{qA}(x_B, Q^2) = 2 e_q^2 \left(\frac{4\pi^2 \alpha_s}{3} \right) \frac{1}{Q^2} x_B \left[\frac{\delta(x_2 - x_B)}{x_1 - x_B} + \frac{\delta(x_1 - x_B)}{x_2 - x_B} \right]. \quad (15)$$

By substituting the above partonic hard parts into Eq. (12), we can derive the leading power corrections to the DIS structure functions defined in Eq. (9).

In order to derive the medium size enhanced power corrections, we need to identify the position space integrals that can be extended freely to the size of the target. For the leading power corrections in Eq. (12), only position space integrals are from the dy_i^- 's in Eq.(13). Generally, these y_i^- integrals cannot grow with the size of the target because of oscillation of the exponential factors. Because of the nature of Fourier transform, the exponentials in Eq. (13) are linear functions of parton momentum fractions. Since the kinematics of inclusive DIS is only sensitive to the total momentum from the target, two of the three momentum fractions in Eq. (12) cannot be fixed by the hard collision. As pointed out in Ref. [11], the integration of these two momentum fractions can be fixed by two unpinched poles from the partonic parts, and the integration removes the oscillation of two exponential factors. Therefore, two corresponding y_i^- integrations can be extended freely to the whole target, and generate the target size enhanced power corrections.

After combining the hadronic matrix element in Eq. (13) with the partonic hard parts in Eq. (14), the momentum fraction x is fixed by the $\delta(x - x_B)$, while dx_1 and dx_2 integrations are dominated by the region where $x_1 \sim x_B$ and $x_2 \sim x_B$, because of the two poles at $1/(x_B - x_1)$ and $1/(x_B - x_2)$ respectively. The fact that two poles are from the matrix element and do not have explicit $i\epsilon$ is an artifact of choosing the light-cone gauge. In order to recover the correct $i\epsilon$ within the light-cone gauge calculations, we adapt the $i\epsilon$ prescription introduced in Ref. [4],

$$\left(\frac{1}{x_B - x_1} \right) \left(\frac{1}{x_B - x_2} \right) \implies \left(\frac{1}{x_1 - x_B + i\epsilon} \right) \left(\frac{1}{x_2 - x_B - i\epsilon} \right). \quad (16)$$

We can also work in a covariant gauge to avoid the spurious poles in the light-cone gauge [13,14]. After carrying out dx_1 and dx_2 integrations, we obtain the leading power corrections to the longitudinal structure function,

$$F_L^A(x_B, Q^2) \Big|_{1/Q^2} = \sum_q e_q^2 4 \left(\frac{4\pi^2 \alpha_s}{3} \right) \frac{1}{Q^2} T_{qF}^A(x_B, Q^2), \quad (17)$$

where \sum_q runs over all quark and antiquark flavors, and the twist-4 quark-gluon correlation function is given by [15]

$$\begin{aligned} T_{qF}^A(x_B, Q^2) &= \int \frac{dy^-}{2\pi} e^{ix_B p^+ y^-} \int \frac{dy_1^- dy_2^-}{2\pi} \theta(y_1^- - y^-) \theta(y_2^-) \\ &\quad \times \langle p_A | \bar{\psi}_q(0) \frac{\gamma^+}{2} F^{+\alpha}(y_2^-) F_\alpha^+(y_1^-) \psi_q(y^-) | p_A \rangle. \end{aligned} \quad (18)$$

In order to derive leading power corrections to F_1 , we expand the x_1 and x_2 in Eq. (15) around x because of the poles in Eq. (13),

$$\frac{\delta(x_2 - x_B)}{x_1 - x_B} + \frac{\delta(x_1 - x_B)}{x_2 - x_B} \approx -\delta'(x - x_B) + \dots \quad (19)$$

where “...” represents terms proportional to powers of $x_i - x$ with $i = 1, 2$. Since these terms cancel the poles in Eq. (13), we can neglect them for calculating the leading nuclear size enhanced contributions, and we obtain

$$F_1^A(x_B, Q^2)\Big|_{1/Q^2} = \frac{1}{2} \sum_q e_q^2 \left(\frac{4\pi^2 \alpha_s}{3} \right) \frac{1}{Q^2} x_B \frac{d}{dx_B} T_{qF}^A(x_B, Q^2), \quad (20)$$

where \sum_q runs over all quark and antiquark flavors, and T_{qF}^A is given in Eq. (18).

In order to estimate the size and sign of the leading power corrections to the structure functions in Eqs. (17) and (20), we need the knowledge of the twist-4 quark-gluon correlation function $T_{qF}^A(x_B, Q^2)$. Although this function is nonperturbative, QCD factorization theorem enables us to find the information on T_{qF}^A from other physical observables. For the following numerical estimate, we adopt the model [15]

$$T_{qF}^A(x, Q^2) \approx \lambda^2 A^{1/3} \phi_{q/A}(x, Q^2), \quad (21)$$

and use $\lambda^2 \approx 0.01 \text{ GeV}^2$ extracted from the Drell-Yan transverse momentum broadening in hadron-nucleus collisions [16]. Substituting T_{qF}^A in Eq. (21) into Eqs. (17) and (20), we find that the leading nuclear size enhanced power corrections to F_L are positive, while the corrections to F_1 are negative. Because of the opposite signs, the nuclear enhanced power corrections to F_2 are smaller.

In order to understand the HERMES data, we consider the following double ratio,

$$R_R \equiv \frac{(1 + \epsilon R_A)}{(1 + R_A)} \Big/ \frac{(1 + \epsilon R_D)}{(1 + R_D)}. \quad (22)$$

Since F_2^A/F_2^D measured by HERMES Collaboration is consistent with the ratio measured by other experiments [1], the double ratio R_R should be responsible for all unique features of HERMES data, such as the x_B , Q^2 , and ϵ dependence of the ratio σ_A/σ_D , defined in Eq. (3). From Eq. (4), we have $R_A = F_L^A/(2F_1^A)$ with the power corrections included for the DIS structure functions

$$F_i^A(x_B, Q^2) = F_i^A(x_B, Q^2)\Big|_{\text{LT}} + F_i^A(x_B, Q^2)\Big|_{1/Q^2} \quad (23)$$

where $i = L, 1$ and “LT” represents the leading twist contributions. The leading power corrections to F_L and F_1 are given in Eqs. (17) and (20), respectively. The leading order leading twist contributions are given in Eqs. (11) and (10), respectively. Since the leading order $F_L^A = 0$ and the order of α_s contributions are renormalization scheme independent, we use them as the nonvanishing contributions to F_L [17]

$$F_L^A(x_B, Q^2)\Big|_{\text{LT}} = \frac{\alpha_s}{2\pi} \left\{ \sum_q e_q^2 \int_{x_B}^1 \frac{dx'}{x'} \phi_{q/A}(x', Q^2) \left[\frac{8}{3} \left(\frac{x_B}{x'} \right) \right] + \left(\sum_q e_q^2 \right) \int_{x_B}^1 \frac{dx'}{x'} \phi_{g/A}(x', Q^2) \left[2 \left(\frac{x_B}{x'} \right) \left(1 - \frac{x_B}{x'} \right) \right] \right\}. \quad (24)$$

Since R_D is well measured and $R_D \approx R_P$ of proton [18], we let $R_D = F_L^D/(2F_1^D)$ with only the leading twist contributions. We find that our R_D in low Q^2 and low x_B region are consistent with the parameterization in Ref. [18]. Because we do not have well-tested parton distributions at Q^2 as low as 0.5 GeV^2 , we will use a set of generic parton distributions in Ref. [19] for the following numerical estimate.

With the model of T_{qF}^A in Eq. (21) and $\lambda^2 = 0.01 \text{ GeV}^2$, and without any further free parameter, we plot the x_B and Q^2 dependence of the double ratio R_R for ^{14}N in Fig. 3(a) and 3(b), respectively. In plotting Fig. 3, we used $E = 27.5 \text{ GeV}$ for the lepton beam energy. In Fig. 3(a), the ratio is sensitive to the value of Q^2 , and $Q^2 = 0.6 \text{ GeV}^2$ was used. In Fig. 3(b), three curves correspond to $x_B = 0.0175$ (dotted), 0.025 (solid), and 0.035 (dashed), respectively. Clearly, Figs. 3(a) and 3(b) reproduce all the key features of the HERMES data shown in Fig. 1 and 2 of Ref. [1]. The detailed numerical comparison with the HERMES data requires better knowledge of original data analysis and reliable low Q^2 parton distributions, and will be presented elsewhere.

In the rest of the Letter, we explain why the nuclear enhanced power corrections are consistent with the HERMES data. As shown in Fig. 3(a) or Fig. 1 of Ref. [1], the ratio R_R or σ_A/σ_D shows a steep falling feature when x_B decreases, which is not observed in other experiments. We find that the steep falling was mainly caused by strong x_B dependence of the ϵ and a large R_A . Substituting $y = Q^2/(2m_N x_B E)$ into Eq. (2), we find that ϵ falls steeply from 0.9 to 0.25 when x_B decreases from 0.03 to 0.0125 at $Q^2 = 0.6 \text{ GeV}^2$. Thus, the ratio $(1 + \epsilon R_A)/(1 + R_A)$ falls along with the ϵ .

The Q^2 dependence, as shown in Fig. 3(b) or in Fig. 2 of Ref. [1], is the most counterintuitive. Normally, when Q^2 increases, we expect the effect of power corrections to go away, or the ratio R_R to approach one. However, the HERMES data shows an opposite behavior. We find that such a counterintuitive behavior in HERMES data was caused by the strong Q^2 dependence of the ϵ parameter. For example, when Q^2 changes from 0.5 GeV^2 to 0.9 GeV^2 , the ϵ at $x_B = 0.0175$ decreases from 0.78 to 0.13 by dropping a factor of 6, while the size of power corrections changes for less than a factor of 2. We find that the decrease of the double ratio R_R when Q^2 increases is due to the steep falling of the combination ϵR_A in Eq. (22).

Similarly, the ϵ dependence of the HERMES data, shown in Fig. 3 of Ref. [1], is a direct consequence of explicit ϵ dependence in Eq. (3) or Eq. (22). From our numerical estimate, we also find that the observed large double ratio $R_A/R_D \sim 5$ for $0.01 < x < 0.03$, as shown in Fig. 5 of Ref. [1], is due to a strongly nuclear enhanced $R_A \sim 1.6$ at $Q^2 = 0.6 \text{ GeV}^2$ and a relatively small $R_D \sim 0.32$, which is consistent with other measurements [18].

We conclude that strong nuclear effects in σ_A/σ_D and R_A/R_D , observed by HERMES Collaboration, are direct consequences of strong nuclear enhanced power corrections. We demonstrated that our numerical estimate reproduces all the features of the HERMES data. When the Q^2 is as small as 0.6 GeV^2 , we find that the structure function $F_1(x_B, Q^2)$ is still dominated by the leading twist contributions, while the longitudinal structure function $F_L(x_B, Q^2)$ is dominated by the nuclear enhanced power corrections. Since the leading power corrections are large, it is therefore important to study the nuclear enhanced power corrections at even higher powers of $1/Q^2$ to have a better QCD prediction.

ACKNOWLEDGMENT

One of us (W.Z.) thanks International Institute of Theoretical and Applied Physics and nuclear theory group at Iowa State University for support and hospitality when this work was initiated. This work was supported in part by the U.S. Department of Energy under Grant Nos. DE-FG02-87ER40731 and DE-FG02-96ER40989, and in part by the National Science Foundation of China 10075020.

REFERENCES

- [1] K. Ackerstaff *et al.*, HERMES Collaboration, Phys. Lett. **B475**, 386(2000).
- [2] B.Z. Kopeliovich, J. Raufeisen, A.V. Tarasov, Phys. Rev. **C62**, 035204(2000); Saul Barshay, Georg Kreyerhoff, Phys. Lett. **B487**, 341(2000); G. A. Miller, S. J. Brodsky, M. Karliner, Phys. Lett. **B481**, 245(2000).
- [3] G. Stermann, *et al.*, CTEQ Collaboration, Rev. Mod. Phys. **67**, 157 (1995).
- [4] A.H. Mueller and J.-W. Qiu, Nucl. Phys. **B268**, 427 (1986).
- [5] J.-W. Qiu, Nucl. Phys. **B291**, 746 (1987).
- [6] P. Amaudruz *et al.*, NMC Collaboration, Phys. Lett. **B294**, 120 (1992); M. Arneodo *et al.*, NMC Collaboration, Nucl. Phys. **B441**, 12 (1995); Phys. Lett. **B481**, 23 (1996).
- [7] J.-W. Qiu and G. Stermann, Nucl. Phys. **B353**, 137 (1991).
- [8] R.K. Ellis, W. Furmanski, and R. Petronzio, Nucl. Phys. **B207**, 1 (1982); **B212**, 29 (1983).
- [9] J.-W. Qiu, Phys. Rev. **D42**, 30 (1990).
- [10] J.-W. Qiu and G. Stermann, Nucl. Phys. **B353**, 105 (1991).
- [11] J.-W. Qiu and G. Stermann, in preparation.
- [12] For example, F. Halzen and A.D. Martin, *Quarks and Leptons – An Introduction Course in Modern Particle Physics*, John Wiley and Sons (1984).
- [13] D. Boer and J.-W. Qiu, hep-ph/0108179.
- [14] M. Luo, J.-W. Qiu, and G. Stermann, Phys. Rev. **D50**, 1951 (1994).
- [15] M. Luo, J.-W. Qiu, and G. Stermann, Phys. Rev. **D49**, 4493 (1994).
- [16] X.-F. Guo, Phys. Rev. **D58**, 114033 (1998).
- [17] R.K. Ellis, W.J. Sterling, and B.R. Webber, *QCD and Collider Physics*, Cambridge University Press (1996).
- [18] L.W. Whitlow *et al.*, Phys. Lett. **B250**, 193 (1990).
- [19] J.-W. Qiu and G. Stermann, Phys. Rev. Lett. **67**, 2264 (1991).

FIGURES

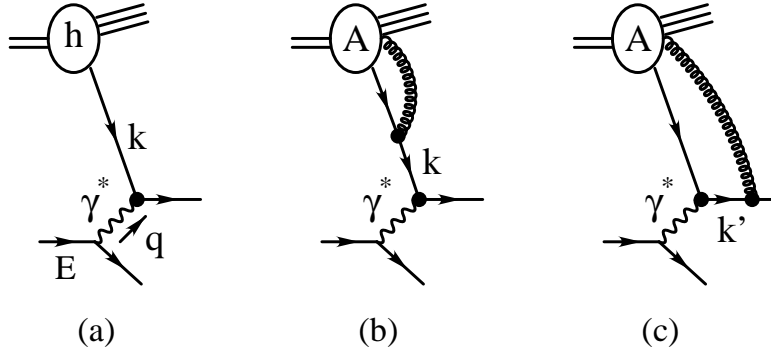


FIG. 1. Sketch for lepton-hadron and lepton-nucleus DIS: (a) single-parton scattering, (b) multiparton interaction internal to the nucleus, and (c) multiparton interaction at the hard collision.

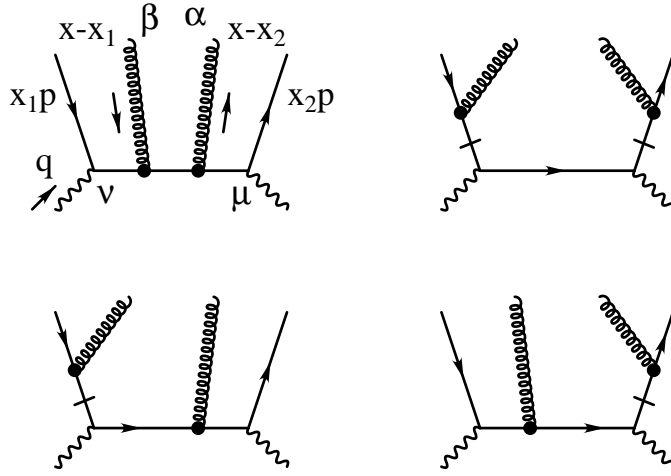


FIG. 2. Leading order Feynman diagrams that contribute to the leading power corrections to the DIS structure functions.

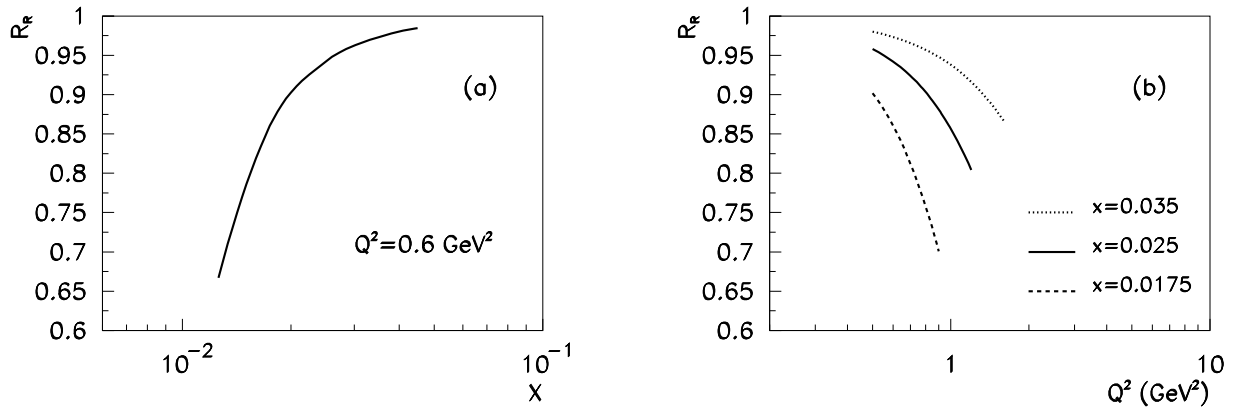


FIG. 3. The double ratio R_R in Eq. (22) as a function of x_B (a) and Q^2 (b). The curves are explained in the text.